Sparse isotropic q-space sampling distribution for Compressed Sensing in DSI

Alexandra Tobisch[1,2], Gabriel Varela[3], Rüdiger Stirnberg[1], Hans Knutsson[4], Thomas Schultz[2,5], Pablo Irarrázaval[3,6], and Tony Stöcker[1]

[1]German Center for Neurodegenerative Diseases (DZNE), Bonn, Germany, [2]University of Bonn, Bonn, Germany, [3]Biomedical Imaging Center, Pontificia Universidad Católica de Chile, Santiago, Metropolitan District, Chile, [4]Linköping University, Linköping, Sweden, [5]MPI for Intelligent Systems, Tübingen, Germany, [6]Department of Electrical Engineering, Pontificia Universidad Católica de Chile, Santiago, Metropolitan District, Chile

INTENDED AUDIENCE Neuroscientists, computer scientists, MR physicists, or related, who are interested in advanced diffusion MRI techniques and fast acquisition of intra-voxel structural parameters

INTRODUCTION Diffusion Spectrum MR Imaging (DSI) provides high angular and radial resolution of intra-voxel microstructure [1], but requires very long acquisition times, not practical for clinical applications. The Compressed Sensing (CS) technique accelerates DSI because it reduces the signal acquisition to fewer randomly distributed q-space samples and recovers the full data through nonlinear reconstruction [2]. State-of-the-art DSI approaches that exploit CS measure diffusion data by applying diffusion gradients distributed on a three-dimensional Cartesian grid [2]. Recently, a method was proposed to generate 3D non-Cartesian sample distributions that aim for isotropic sampling of q-space [3]. The approach extends the electrostatic repulsion algorithm used for q-ball imaging [4]. In this work we show the advantages of such isotropic sampling patterns over the conventional Cartesian sampling in sparse reconstructions.

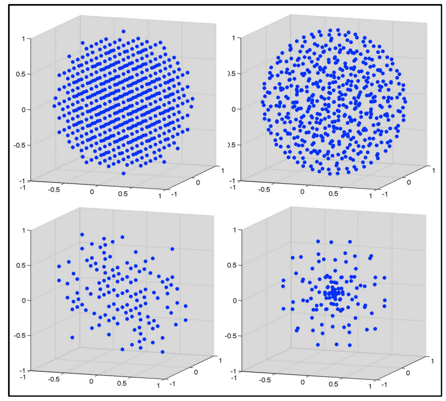

Fig. 1. Nyquist (upper row) and sparse (lower row) q-space sampling: 514 Cartesian samples (top left), 514 isotropic samples (top right), 128 Cartesian samples (bottom left), 128 isotropic samples (bottom right)

METHODS We use the Camino Monte-Carlo simulator [5] to generate noise-free pulsed gradient spin echo [6] diffusion signals (q_{max} = 65.507mm^{-1}, g_{max} = 26.79mT/m, δ = 57.4ms, Δ = 65.9ms) for 514 samples distributed on a Cartesian 11x11x11 q-space grid and for an isotropic sample distribution of the same size (Fig. 1, upper row). Both patterns give full q-space coverage and provide the ground truth to evaluate the reconstruction results. Accelerated DSI acquisitions are simulated by drawing random samples from the Nyquist Cartesian sampled data, with Gaussian probabilities as in [2]. With the Camino simulator, we create diffusion signals based on an isotropic undersampling scheme [3] generated with the metric T-21112 and a charge density of r^{-2} to sample more densely in the center of q-space. Both undersampling patterns acquire 128 q-space samples corresponding to an acceleration factor of 4 (Fig. 1, lower row). Diffusion signals for one voxel containing two fiber bundles with a crossing angle of 55° are simulated. We further vary the 3D orientation of the crossing structure by fixing the rotation about the x-axis to 35° and rotating about the y-axis by 5°-175° in 10° steps. We use the CS approach by Lustig et al. [7] and extend it to express the relationship between three-dimensional q-space data and the diffusion propagator via nonuniform FFT [8]. For a fair comparison that evaluates the reconstruction quality based on the sampling pattern, all simulated data are processed with the CS algorithm using nonuniform FFT. Four different metrics are used to evaluate the deviation of the reconstruction from the ground truth: the root-mean-square error (RMSE), the return-to-origin probability (p0), the angular displacement and a measure of geometrical sharpness of peaks in the orientation distribution function (ODF) [9]. For each metric, we calculate the mean and standard deviation of the error values obtained for the 18 different orientations of the crossing fiber structure.

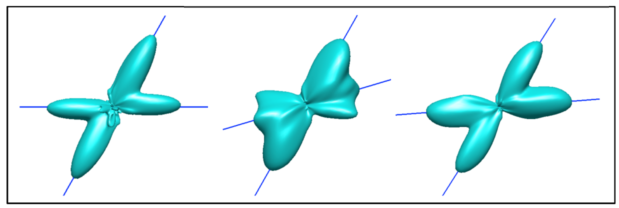

Fig. 2. ODF of the ground truth (left) and ODF after CS obtained for Cartesian sampling (middle) and isotropic sampling (right); the crossing structure is rotated 35° and 95° about the x- and y-axis, respectively

Sampling	RMSE	Δp0	Δφ	sharpness
Cartesian	$0.0016 \pm 9.01 * 10^{-5}$	0.0264 ± 0.011	4.25 ± 3.16	0.9501 ± 0.1436
Isotropic	$0.0013 \pm 8.36 * 10^{-5}$	0.0052 ± 0.003	3.34 ± 1.65	1.2872 ± 0.1207

Table 1. Mean and standard deviation for all metrics over all orientations of the crossing structure: the root-mean-square error (RMSE), the deviation from the return-to-origin probability of the ground truth (Δp0), the angular displacement from the ground truth (Δφ) and the ODF sharpness

RESULTS AND DISCUSSION For simulated DWI data, the reconstruction obtained with isotropic sampling outperforms the one using Cartesian sampling. For each metric, table 1 shows the mean and standard deviation calculated for 18 different orientations of the crossing fiber structure. For the isotropic sampling, the RMSE and the return-to-origin probability are closer to the ground truth and the increased sharpness compared to the Cartesian sampling emphasizes the sharper reconstruction of the crossing structure. The angular displacement of the reconstructed fibers is lower for the isotropic sampling scheme. Fig. 2 visualizes the ODF for the ground truth and the ODF of the diffusion propagator obtained after applying the CS algorithm and shows superior quality when using a sampling distribution by [3]. The results show that acquiring q-space data with an isotropic sample distribution rather than a Cartesian one captures better the diffusion profile, which improves sparse reconstructions.

CONCLUSION This work demonstrates the suitability of the q-space sampling distributions introduced by [3] for Compressed Sensing in DSI. Sparse data acquisition with isotropic q-space sampling provides better reconstruction results than conventional Cartesian sampling applied in most state-of-the-art CS applications. Future work will apply these sampling patterns to phantom imaging data and in-vivo MR scans.

ACKNOWLEDGEMENT This work was supported by BMBF grant 01DN1306, NIH grants P41EB015902, R01MH074794, and Swedish Research Council grant 2012-3682.

REFERENCES [1] Wedeen et al. MRM 2005; [2] Menzel et al. MRM 2011; [3] Knutsson and Westin. MICCAI 2013; [4] Jones et al. MRM 1999; [5] Hall and Alexander. IEEE TMI 2009; [6] Stejskal et al. JCP 1965; [7] Lustig et al. MRM 2007; [8] Fessler and Sutton. IEEE TSP 2003; [9] Schultz and Kindlmann. CGF 2010;